

# An integrated procedure to assess knee-joint kinematics and kinetics during gait using an optoelectric system and standardized X-rays

J. Li, U.P. Wyss\*, P.A. Costigan\* and K.J. Deluzio\*

King Faisal Specialist Hospital and Research Centre, MBC 77, Riyadh, 11211, Saudi Arabia;  
\*Clinical Mechanics Group and Department of Mechanical Engineering, Queen's University, Kingston, Ontario, Canada K7L 3N6

Received August 1992, accepted March 1993

## ABSTRACT

*This paper describes a 3-D gait analysis system, which combines optoelectric motion tracking and a standardized X-ray procedure, to calculate the net knee-joint forces and moments of a normal subject group during walking. The optoelectric system collects kinematic data from infra-red LED markers placed at selected skin surface locations and projecting probes attached to the lower limb. A standardized X-ray procedure is used to move surface markers into their designated bony landmarks based on individual bone structure, which reduces the error caused by uncertainty of skin-surface marker locations. Based on moved-in marker information, different joint coordinate systems are proposed for kinematic and kinetic analysis of the knee joint. Normalized data of knee angles, net reaction forces and net moments from 35 young, normal subjects are presented.*

**Keywords:** Knee joint, gait analysis, three-dimensional (3-D), inverse dynamics approach, joint reaction force, net moment, Cardan angles, floating axis

## INTRODUCTION

Although much research has been conducted to study the knee-joint dynamics during gait, there is no practical method which can measure directly the internal forces generated by muscles, ligaments and other soft tissues surrounding the knee. Their resultants can only be estimated from observed segmental kinematics and measured external forces. This reversed procedure was referred to as the 'inverse dynamics problem'<sup>1</sup>, in which segmental displacement data were differentiated twice to obtain acceleration data. After inertial properties of the segment were estimated, joint kinetic resultants could be calculated since they were the only unknowns in equations of motion. Bresler and Frankel<sup>2</sup> were the first to use the 'inverse dynamics approach' to calculate the net reaction forces and moments at the hip, knee and ankle joints during normal level walking. However, the graphical differentiation method they had to use was time-consuming and highly susceptible to magnifying the inherent experimental error in raw displacement data. Using a numerical differentiation procedure incorporating a form of smoothing, Morrison<sup>3,4</sup> also evaluated the net reaction forces and moments at the knee joint. None-the-less, the accuracy of the study was still unknown

as he failed to give the error estimates of either kinematic or kinetic results. Harrington<sup>5</sup> modified Morrison's method to examine the stance phase of gait during normal and pathological situations. By ignoring the effects of gravitation and inertia completely, he was able to avoid the differentiation process and still obtained the peak forces in the same orders of magnitude as those calculated by Morrison.

It was not until the late 1970s that new technology enabled researchers to explore the full potential of the 'inverse dynamics approach'. Developments in computer technology and optoelectronic devices not only enhanced the speed and accuracy of data collection, eliminated tedious manual processing (e.g. by use of digitization), but also upgraded the gait-data collection and processing from two-dimensional or pseudo-three-dimensional to truly three-dimensional<sup>6-8</sup>. Additional theoretical and experimental work based on the 'inverse dynamics approach' has appeared in the literature<sup>9-15</sup>.

Unfortunately, optoelectronic devices still have to rely on skin-surface markers to measure body-segment positions. Therefore, like most motion tracking systems, they suffer from two sources of error: relative movements between markers and underlying bones (skin motion), and uncertain positions between external markers and internal bony landmarks<sup>16</sup>. Although these errors may be eliminated by the use of cortical pins fixed directly into the human bones<sup>16</sup>, it is achieved at the expense of physical

Correspondence and reprint requests to: Dr. Urs Wyss, Clinical Mechanics Group, Apps Medical Research Centre, Kingston General Hospital, Kingston, Ontario, Canada K7L 2V7

© 1993 Butterworth-Heinemann for BES  
0141-5425/93/05392-09

discomfort for the subject. Furthermore, surface markers placed on the side of the joint do not coincide with the anatomical joint endpoint in 3-D space. These markers must be moved 'into' the segment medially in the frontal plane to coincide with the joint endpoint. Previously in most studies<sup>8,10</sup> the surface markers were simply moved 'into' the middle of the segment at the level of the marker to represent the segment endpoints, which did not take into consideration any individual bone shape differences, nor did it consider the error associated with identifying the bony landmarks from the skin surface. The potential error could hinder the reliability of the final kinematic and kinetic results.

In the evaluation of joint kinematics and kinetics, it is also important to choose appropriate joint coordinate systems. Euler angles, the floating-axis method and Cardan angles have been proposed to describe the rotational movement of a 3-D joint in space<sup>17-19</sup>, but not all of them can be used directly for kinetic analysis. The screw-axis (or helical-axis) method, also proposed for the description of human joints<sup>20</sup>, serves mainly as a landmark for kinematic reference of the joint<sup>21</sup>. Its use for clinical description of joint angles is not as popular as the three previously mentioned methods.

The purpose of the current study was to develop an integrated gait-analysis system which combines an optoelectric motion-tracking system and a standardized X-ray procedure to evaluate the individual loading patterns at the knee during gait. It aimed at minimizing the two previously mentioned error sources by identifying the precise relationship between surface markers and corresponding bony landmarks. This paper describes the detailed methodology including marker 'moving-in' technique and description of the joint coordinate system and governing equations, and presents 3-D data on joint angles, net forces and moments at the knee of a young, normal subject group during walking. A sensitivity analysis was also conducted to evaluate the potential error caused by incorrect bony landmark identification.

## METHODOLOGY

Kinematic data were collected with a two-camera optoelectric system (WATSMART from Northern Digital, Waterloo, Ontario), which uses infra-red light-emitting diodes (LEDs) as surface markers. Two cameras were mounted on tripods in such a way that their field of view covered one complete gait cycle. Care was taken to minimize reflections, as they result in the erroneous detection of LEDs. The ceiling and walkway were painted flat black, with nonreflective carpet placed in front of the walkway. Black fibrous curtains were hung behind the walkway, and the windows were covered to eliminate sunlight.

A global coordinate system was set up and aligned to the edges of the force platform (AMTI from Advanced Mechanical Technology, Inc., Newton, MA), which was mounted in the middle of the walkway. The X-axis is in the forward walking direction of the walkway, the Y-axis is at a right angle to the direction of the walkway, and the Z-axis is

**Table 1** Subject characteristics ( $N = 35$ )

	Mean	SD	Minimum	Maximum	Range
Height (cm)	172.0	7.5	152.0	191.5	39.5
Weight (kg)	65.4	11.1	46.0	98.5	52.5
Age (yr)	24.6	2.7	19.7	29.9	10.2
Velocity ( $\text{m s}^{-1}$ )	1.17	0.13	0.94	1.53	0.59

pointing upwards, perpendicular to the force platform.

The accuracy of the whole motion-tracking system in the testing configuration was evaluated both kinematically and kinetically using various mechanical models<sup>22</sup>. Two simple mechanical models with known behaviour were used to assess the system performance, both simulating elements of the human knee: the first represented the three clinical rotations of the knee, while the second allowed accurate force measurements of a single-degree-of-freedom link. Flexion-extension and longitudinal rotation could be measured within 2°, with the error in abduction-adduction slightly higher (4°). Deluzio *et al.*<sup>22</sup> also demonstrated that LEDs should be placed at least 20 cm away from each other to achieve maximum accuracy. Inertial force calculations were accurate within 8.0%.

A total of thirty-five young healthy subjects took part in this study. All of them were between the ages of 20 and 30, and had no previous knee injuries or abnormalities. *Table 1* shows the statistics for height, weight, age and walking speed of the 35 subjects. Data for level walking were collected for one stride cycle, which is the time between two consecutive initial foot contacts of the same foot. The initial foot-contact instances were determined by a footswitch, which was placed at the subject's heel.

## Surface-marker positioning and 'moving-in'

Since the motion of the leg is limited during the stance phase of the gait cycle, surface markers placed at bony spots with less soft tissue between the marker and underlying bone will be much less affected by the skin and soft-tissue motion. In the present study, two positions at each end of the femur and tibia were selected: greater trochanter, lateral femoral epicondyle, head of fibula and lateral ankle malleolus. As a minimum of three markers was required to define the orientation of each segment, a third marker was placed on the projecting probe attached to each segment, in order to assure a distance of 20 cm or more between each marker (*Figure 1*). The error caused by probe vibration is mostly of high frequency and can be filtered out by a regular low-pass filter.

The four surface markers, however, must be not only placed accurately at designated bony landmarks for each subject, but also moved medially 'into' the segment in the frontal plane, so that the represented limb endpoint would be accurate in three-dimensional space. A special procedure was developed utilizing a standardized radiographic technique (QUESTOR Precision Radiography (QPR), Clinical Mechanics Group, Queen's University, Ontario) to fulfil this purpose<sup>23</sup>.

The normal standing radiograph, which provides a

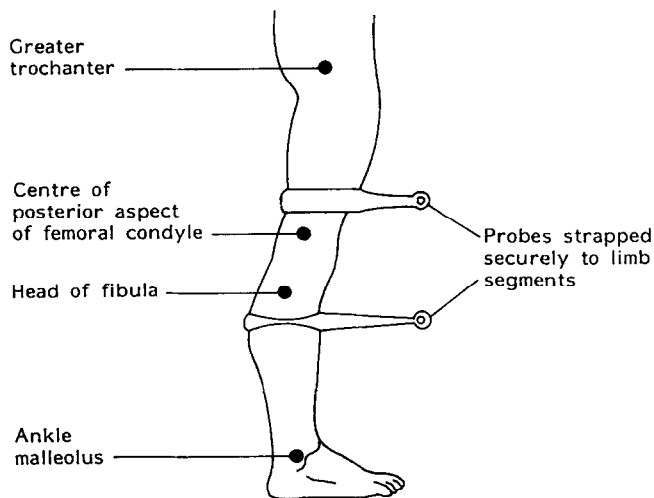


**Figure 1** Location of markers on subject, LEDs are placed on easily identifiable bony landmarks. A third LED per segment is attached to rigid extensions of each segment

view of the knee only, is prone to errors of parallax and poor control of patient positioning. QPR provides a frontal view of the hip, and frontal and sagittal views of the knee, with the ankle position known and standardized. The subject stands in a rotating template within a frame bearing radio-opaque markers, which allows for standardization of each X-ray view and correction for parallax error. It has been employed as part of the routine pre- and post-

operative assessment of all osteotomy and knee-replacement cases at the Kingston General Hospital for more than six years. A full description of the QPR procedure and an extensive error analysis has been published<sup>24</sup>.

Once all LED surface markers were positioned and the probes attached, a single motion trial was performed with the subject standing in a static reference position (*Figure 2*). The reference position was defined by the subject's foot-rotation angle measured against the protractor scale on the template. The template, which is the same as the one in the QPR frame, was also aligned with the edges of the force plate. After the motion data were collected, the surface markers were removed and replaced with small lead shots. The subject then underwent the routine clinical QPR procedure. In the QPR frame, the subject rotated his/her foot to the same angle as that recorded during the motion trial, which ensured that the subject stood in the same orientation in both the QPR frame and the global coordinate system. As the result, the X-ray views provided precise locations of the surface markers with respect to the knee's internal structure in the global coordinate system (*Figure 3*).

Once QPR X-rays have been digitized, the data can be scaled and the vectors that move the surface marks 'into' the segment can be defined. The initial correction vector for the ankle marker was a vector parallel to the Y-axis. To adjust for foot rotation, the resultant ankle correction vector was obtained by

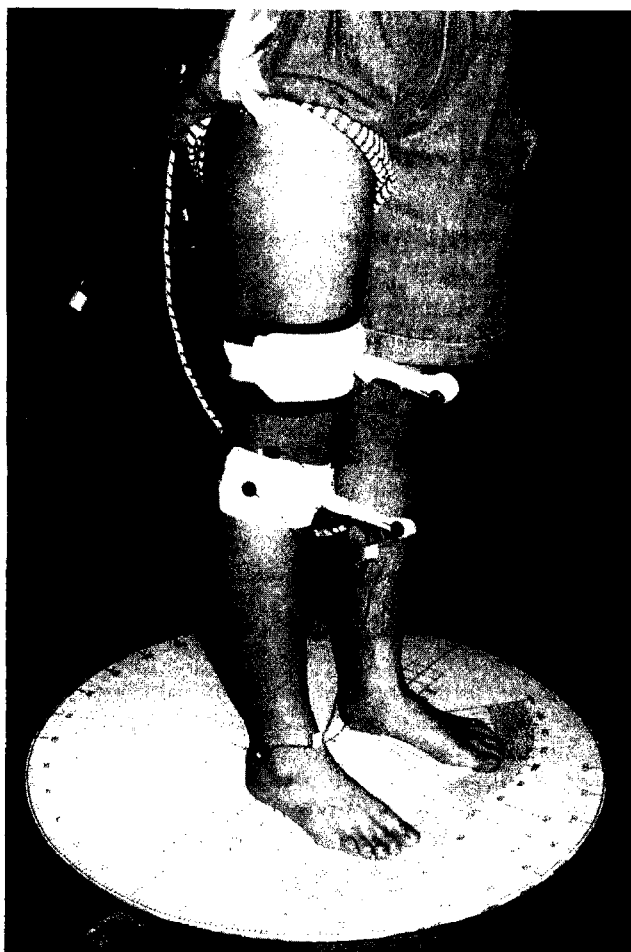


**Figure 2** Subject fitted with instruments, standing in the reference position



**Figure 3** QPR X-rays of the sagittal and frontal views of the knee joint. In the frontal view, two surface markers on the side clearly demonstrate the necessity of moving the markers 'into' the segment. Other markers shown on the sagittal picture are radio-opaque markers which are used to correct the image from parallax error

rotating the initial vector about the Z-axis by the amount of external foot rotation measured from the QPR template. The marker was then moved along the correction vector, 'into' the ankle a distance of one-half of the ankle width. The greater-trochanter marker was moved to the estimated hip-joint centre along the vector from the trochanter marker to the hip centre. Similarly, the marker at the head of the fibula was moved to the top of the intercondylar eminence of the tibia. Finally, the femoral-epicondyle marker was moved to the approximate centre of the posterior condyle of the distal femur. Corrections were made in both sagittal and frontal planes.

Although correction vectors were defined with respect to the global system, they could be easily transformed into the body-fixed coordinate system for each segment. Now that correction vectors are fixed within each body-fixed coordinate system, the surface-marker coordinates can be adjusted by shifting them along the respective correction vectors at any point in time, regardless of the position of the limb. By moving the surface markers 'into' the same designated bony landmarks for each subject, errors resulting from uncertainty of surface-marker locations with respect to bony landmarks can be reduced significantly.

### Cardan angles and body-fixed coordinate system

Among several methods available to describe the rotational movement of the joint, Euler angles defined by Chao<sup>17</sup> are not conventional Euler angles because the first axis of rotation is fixed on the femur, the last fixed on the tibia, and the second floating. In fact, they are the same angles as the floating-axis angles defined by Grood and Suntay<sup>18</sup>. Kinematically, the use of these angles is advantageous as they can be obtained regardless of the sequence of rotation. However, both methods cannot be used directly for kinetic calculations, since three rotational angles describe the relative positions of two segments in space. In order to apply kinetic equations, Cardan angles proposed by Tupling and Pierrynowski<sup>19</sup> are convenient as they follow the conventional definition of Euler angles, which define the absolute orientation of one segment in space. More comparisons of the three methods are given in Appendix A.

Since the forces acting upon the ankle joint are not the concern of the study, the foot and shank were considered as one segment. In order to locate the foot and shank position in 3-D space, three orthogonal, body-fixed coordinate axes fixed on the shank were defined on the basis of two surface markers and one marker at the end of the projecting probe. The 'moved-in' markers at the head of the fibula and lateral ankle malleolus were used to define the long axis of the tibia, which points from distal to proximal (DP) direction. The marker at the end of the projecting probe attached to the tibia can be aligned with the fibula marker to define the posterior-anterior (PA) direction. The lateral-medial (LM) axis was obtained from the cross-product of the previous two vectors. The origin of the body-fixed coordinate system was set at the estimated centre of mass of the foot and shank.

Three body-fixed axes combined with three space-

fixed global coordinate axes define a set of Cardan angles,  $\alpha$ ,  $\beta$ ,  $\gamma$ , which are expressed as follows:

$$\beta = \arcsin(-\vec{e}_2 \cdot \vec{K})$$

$$\alpha = \arcsin(\vec{e}_1 \cdot \vec{K} / \cos \beta)$$

$$\alpha = \alpha \quad \text{if } \vec{e}_3 \cdot \vec{K} > 0$$

$$\alpha = \pi - \alpha \quad \text{if } \vec{e}_3 \cdot \vec{K} < 0$$

$$\gamma = \arcsin(\vec{e}_2 \cdot \vec{I} / \cos \beta)$$

$$\gamma = \gamma \quad \text{if } \vec{e}_2 \cdot \vec{J} > 0$$

$$\gamma = \pi - \gamma \quad \text{if } \vec{e}_2 \cdot \vec{J} < 0$$

Where  $\vec{e}_1$ ,  $\vec{e}_2$ ,  $\vec{e}_3$ , and  $\vec{I}$ ,  $\vec{J}$ ,  $\vec{K}$  are the unit vectors of three body-fixed coordinate axes and three global coordinate axes respectively<sup>26</sup>.

The three Cardan angles defined above, however, do not represent the flexion-extension, abduction-adduction and internal-external rotation angles of the knee joint; instead, they describe the 3-D orientation of the tibia in the global coordinate system. Furthermore, three components of the angular velocity of the segment cannot be obtained by a simple differentiation of three Cardan angles, as was normally the case in 2-D situations. Their expressions in the body-fixed coordinate system are given as follows<sup>27</sup>:

$$\omega_1 = \dot{\alpha} \cos \beta \sin \gamma + \beta \cos \gamma$$

$$\omega_2 = \dot{\alpha} \cos \beta \cos \gamma - \beta \sin \gamma$$

$$\omega_3 = -\dot{\alpha} \sin \beta + \dot{\gamma}$$

Time differentiation of  $\omega_1$ ,  $\omega_2$ ,  $\omega_3$  here would provide corresponding angular accelerations.

In order to obtain flexion-extension, abduction-adduction, and internal-external rotation angles at the knee joint, another body-fixed coordinate system was defined on the femur based on 'moved-in' markers at the greater trochanter and femoral epicondyle, and the marker at the end of the projecting probe attached to the thigh. The floating-axis method was used to calculate three clinical angles.

### Equations of motion

If the foot and shank are considered symmetrical longitudinally, three body-fixed coordinate axes also represent the three principal moment-of-inertia axes. But only two different principal moment-of-inertia values ( $I_{11}$  and  $I_{33}$ ) exist, the third one ( $I_{22}$ ) being equal to  $I_{11}$ . The value of  $I_{11}$  is available in the literature<sup>28</sup>.  $I_{33}$  was estimated from the data provided by McConville *et al.*<sup>29</sup>. The mass and centre-of-mass of the foot and shank were estimated from the regression equations provided by Clauer *et al.*<sup>30</sup>. Finally, the net joint-reaction forces and net external moments at the proximal end of the tibia can be calculated. More details may be found in Appendix B. Figure 4 shows the flow of the integrated procedure.

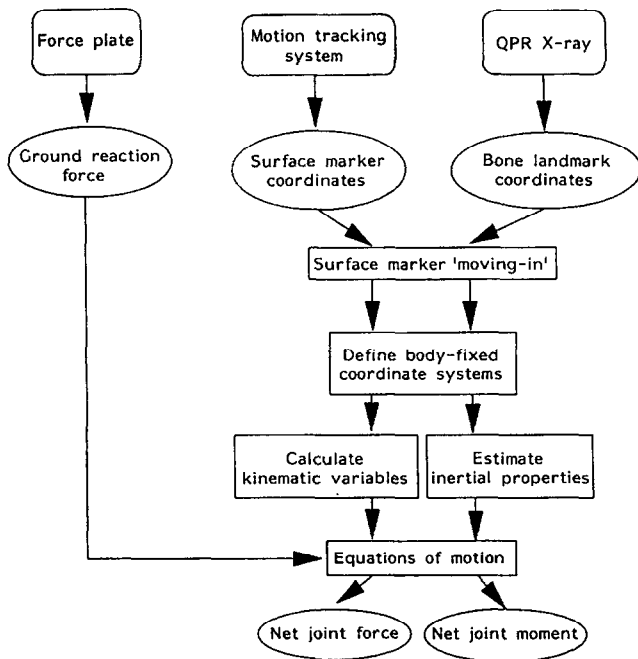


**Figure 4** Flow chart of the inverse dynamics approach combined with surface marker 'moving-in' technique

**Data collection and processing**

Overall, the data collection sequence ran as follows. The four anatomical landmarks were identified and marked, and the QPR was performed. The subject was then fitted with the footswitch, the limb probes and the LED markers. The static reference position

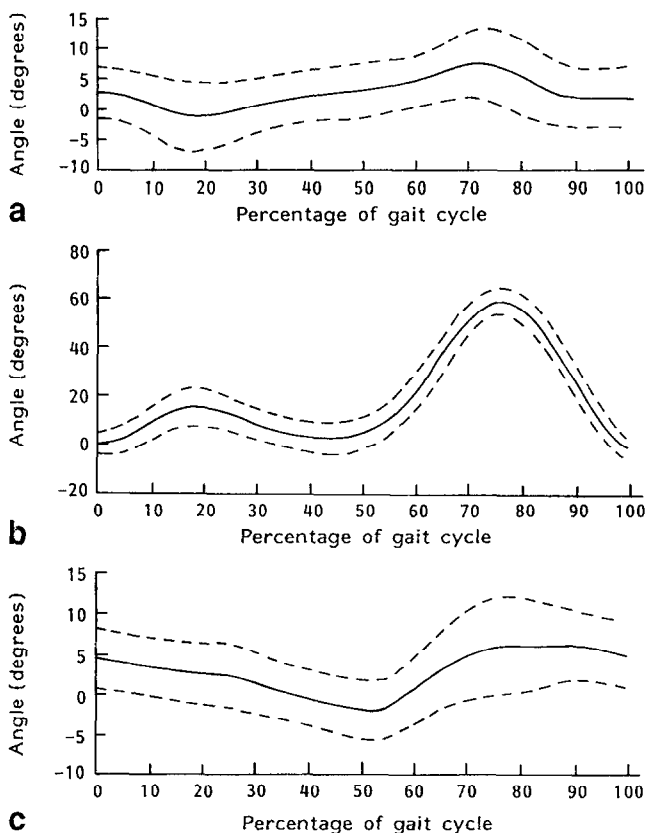


**Figure 5** Relative knee angles of **a**, abduction; **b**, flexion; and **c**, external rotation in 35 young normal subjects. The solid line shows the mean while the dashed lines show plus or minus one standard deviation

was collected, and the motion trials were begun. After a series of walking trials, the collection process was interrupted, and the trials were checked. Trials with clean force plate data, accurate footswitch signals and acceptable missing markers were saved until five of these 'good' trials were collected. The anthropometric data were then recorded.

All software required for the collection and 3-D reconstruction of LED markers was supplied with the optoelectric system<sup>31</sup>. A semi-automatic 3-D knee-motion assessment system was developed to speed up the data-processing efficiency<sup>23</sup>. Once the QPR X-rays have been digitized and the anthropometric measures recorded, the collected motion data can be processed and output files produced without user intervention.

**RESULTS**

All kinematic and kinetic data obtained from every walking cycle for each subject were normalized from initial heel contact to the next heel contact of the same foot. The mean data for each subject were computed by averaging five complete cycles and normalizing by his/her body mass.

Figure 5 shows the average clinical knee angles, plus or minus one standard deviation, of 35 subjects during normal level walking. The three graphs show flexion-extension, abduction-adduction, and external-internal rotation angles with flexion, abduction and external rotation being positive.

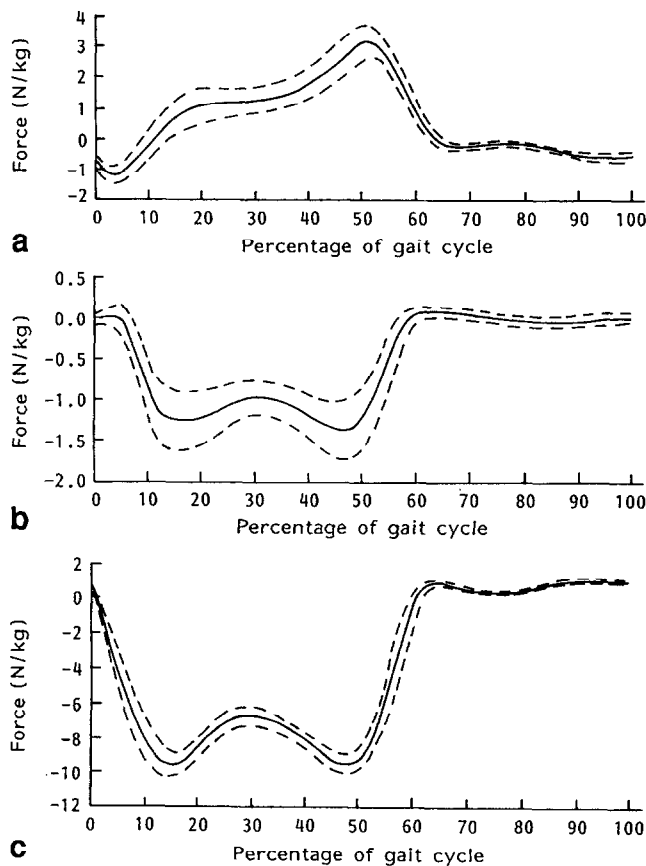


**Figure 6** Net reaction forces of 35 young, normal subjects expressed in the body-fixed coordinate system. All forces (*N*) were normalized by subject's bodymass (*kg*). The solid line shows the mean while the dashed lines show plus or minus one standard deviation. **a**, from posterior to anterior direction; **b**, from lateral to medial direction; **c**, from distal to proximal direction

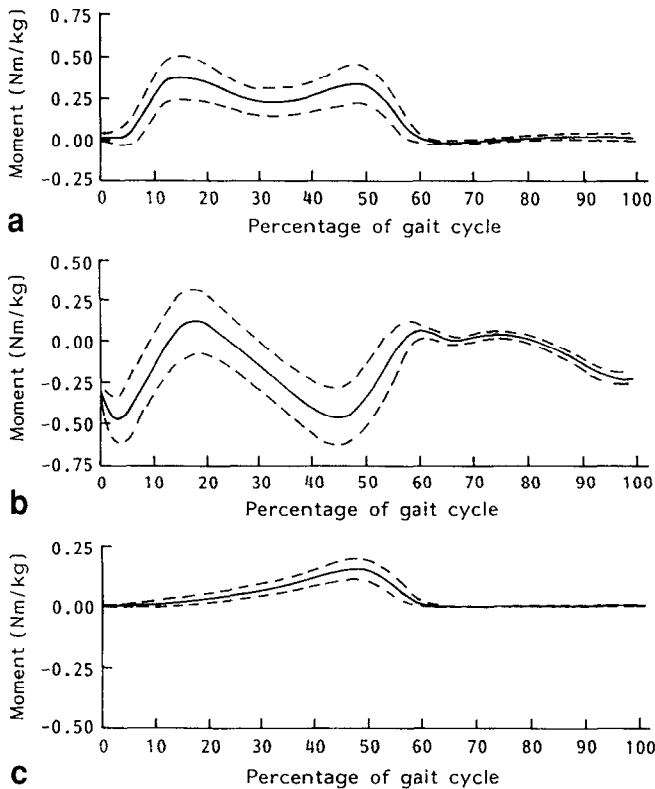


**Figure 7** Net external moment of 35 young, normal subjects expressed in the body-fixed coordinate system. All moments (Nm) were normalized by subject's bodymass (kg). The solid line shows the mean while the dashed lines show plus or minus one standard deviation. **a**, PA-axis component of the moment (frontal); **b**, LM-axis component of the moment (sagittal); **c**, DP-axis component of the moment (transverse)

Figures 6 and 7 show average net joint-reaction forces and moments at the knee, plus or minus one standard deviation, of 35 subjects during normal level walking. In Figure 6, the three graphs show the force values in posterior–anterior (PA), medial–lateral (ML), and distal–proximal (DP) directions respectively. In Figure 7, the three graphs show the moment values in frontal, sagittal, and transverse planes respectively.

## DISCUSSION

A summary of the knee-joint angle data (range of motion) from the present study along with the data from some previous studies are compared in Table 2.

In all studies, the flexion–extension angle has the most consistent pattern during gait cycle. The results from the current study agree well with those of previous studies both in range and shape. For the abduction–adduction and internal–external rotation angles, however, none of the previous studies showed

consistent data. Sensitivity analysis by Kadaba *et al.*<sup>8</sup> showed that errors in abduction–adduction and internal–external rotation angles were mainly due to the uncertainty in the construction of the body-fixed coordinate system, which may be caused either by different coordinate axis definitions, or by errors in locating the true rotation axes. For example, if the actual flexion–extension motion did not take place about its defined axis, the computed knee angles would be in error. Kadaba *et al.* showed that while the knee flexion–extension angle was relatively unaffected by this effect, abduction–adduction and rotation angles were affected non-uniformly throughout the gait cycle. Pennock and Clark<sup>35</sup> showed that abduction–adduction and rotation angles were affected most at the maximum knee flexion. There were differences of 7° in abduction–adduction angle and 8° in internal–external rotation angle between the coordinate systems proposed by Grood and Suntay<sup>18</sup> and Pennock and Clark<sup>35</sup>, whereas the difference for flexion–extension angle was only 1°. Therefore, abduction–adduction and internal–external rotation angles should be interpreted with caution. Locations and orientations of proposed coordinate axes must be defined clearly. It is also desirable to define a set of standardized joint coordinate systems so that results among different laboratories can be compared directly. For now, it may be more appropriate to compare only the range of motion rather than the absolute values among different studies. Although skin-surface markers were used in this study, all three curves in Figure 5 compared favourably in both shapes and ranges with those of Lafortune *et al.*<sup>16</sup>, who utilized cortical pins to assess knee joint kinematics.

Kadaba *et al.*<sup>12</sup> found that patterns of forces and moments during gait were quite repeatable. A pilot study<sup>36</sup> conducted in the same experimental environment as this study showed body-fixed terms had higher repeatability values than those of the global terms. Since each individual has his/her own body-fixed axes, forces and moments should be expressed in the body-fixed coordinate system in order to demonstrate any individual characteristics.

Net forces presented in this paper are the reaction forces of the knee to the external forces acting on the foot and shank. Clinically, net joint forces can sometimes be used to detect differences between normal and abnormal walking patterns. More importantly, they are necessary for the calculation of other important parameters such as joint moments and bone-on-bone forces.

Net moments presented were the sum of those generated by external forces, including the ground reaction force at the foot, net joint force at the

**Table 2** Comparison of ranges of motion of knee joint angles (°) with previous work

Investigators	Techniques	N	Age	F/E	A/D	Rot.
Present study	WATSMART System	35	20–30	60.9	8.7	8.2
Lafortune <i>et al.</i> <sup>16</sup>	Intracortical pins	5	27	60.5	5.2	9.4
Kadaba <i>et al.</i> <sup>8</sup>	Vicon	40	18–40	56.7	13.4	16.0
Isacson <i>et al.</i> <sup>32</sup>	Goniometer	20	25–35	60.6	9.0	12.9
Chao <i>et al.</i> <sup>33</sup>	Goniometer	110	19–32	68.0	10.0	13.0
Winter <i>et al.</i> <sup>34</sup>	Film	16	—	64.0	—	—

N: number of subjects; F/E: flexion–extension; A/D: abduction–adduction; Rot.: internal–external rotation

proximal end of the tibia, and inertial forces of the foot and shank. The signs of moments were decided by the right-hand screw method, with the direction of the axis given for each graph. An internal moment, which is generated by muscles, ligaments and other soft tissues, is required to balance this external moment. For example, if the net moment in the sagittal plane is positive, it will tend to flex the knee. To resist this motion, the main generator of the extensor moment, the quadriceps, must generate a certain amount of force. Winter<sup>37</sup> also presented the net sagittal moment data of 19 subjects with natural cadence. He used a simple 2-D link segment model and did not adjust for surface-marker positions. Despite a smaller number of subjects, his data had larger standard deviations than the moment data shown in the middle graph of *Figure 7*.

Since the era of Bresler and Frankel<sup>2</sup>, the knee-joint rotation centre was selected as the moment-balance point in the majority of studies. From a dynamics point of view, however, the simple moment equations are derived with respect to either a fixed point, the centre of mass of the segment, or the instantaneous rotation centre of the segment in space. The knee-joint centre is the instantaneous rotation centre of the tibia with respect to the femur, so moment equations based on it are more complicated (Appendix B). Furthermore, the joint centre is no longer a definable point in 3-D situations where it is more appropriate to use the instant axis concept. Therefore, it is preferable to choose the centre of mass as the moment-balance point.

The knee-joint rotation centre is still a valuable point to estimate since the joint-reaction force passes through it. It is not only required to calculate the moments generated by the joint-reaction force, but also used as a base point to measure the moment arms of major muscle groups in any attempt to evaluate muscle forces. Although much research has been carried out to determine the instant rotation centre of the knee, no technique has been accepted by most researchers as the optimal and standard procedure. In this study, the rotation centre was chosen to be the one estimated by Nietert<sup>38</sup>, who found that the location of the average centre of rotation for normal subjects was roughly in the centre of the posterior part of the femoral condyles. It is approximated by the surface marker on the lateral femoral condyle, which was later moved into the proposed position using the X-ray based surface marker 'moving-in' technique detailed previously.

Besides system errors from the motion-tracking system and QPR X-ray procedure, several error sources affect the accuracy of the resultant kinematic and kinetic data to various degrees. They include: bony landmark identification; non-symmetry of the foot and shank; estimation of mass and centre of mass of the foot and shank, shoe effect, etc. A sensitivity analysis<sup>39</sup> showed that the accurate identification of bony landmarks was crucial for the accuracy of final kinematic and kinetic results. Even with the marker 'moving-in' technique, the potential error could still be large. For example, a 3 mm deviation of the X-axis coordinate for the determination of intercondylar eminence of the tibia would result in about a 10% change in the peak of the sagittal moment. Without

the marker 'moving-in' procedure, the error could be well beyond the 10% level. The sensitivity analysis also showed that the final results were relatively insensitive to inertial changes during the stance phase of the gait cycle. Only during the swing phase of the gait cycle were the final results able to show differences due to inertial changes.

## CONCLUSIONS

This paper has described how the optoelectric motion-tracking system and standardized QPR X-ray procedure can complement each other to provide an accurate technique to evaluate the individual loading patterns at the knee during gait. The optoelectric system collected kinematic data from infra-red LED markers placed at selected skin-surface locations and projecting probes attached to the lower limb to reduce the skin motion. The QPR X-ray procedure was used to move surface markers 'into' their designated bony landmarks based on individual bone structure, which reduced the error caused by the uncertainty of location of the skin-surface markers relative to their bony landmarks. Normalized knee angles, net forces and net moments of 35 young, normal subjects were presented. In the future, an immediate extension of this study may be the estimation of bone-on-bone forces at the tibia plateau. If muscular moments can be predicted adequately with calibrated electromyography signals, the muscle forces can be calculated as QPR can be utilized to recognize the muscle alignment. Thus bone-on-bone forces at the tibia plateau surface may be estimated.

## REFERENCES

1. Chao EYS, Rim K. Application of optimization principles in determining the applied moments in human leg joints during gait. *J Biomech* 1973; **6**: 497-510.
2. Bresler B, Frankel JP. The forces and moments in the leg during level walking. *Trans ASME* 1950, **Jan**; 27-36.
3. Morrison JB. Bioengineering analysis of force actions transmitted by the knee joint. *Biomed Eng* 1968; **4**: 164-70.
4. Morrison JB. The mechanics of the knee joint in relation to normal walking. *J Biomech* 1970; **3**: 51-61.
5. Harrington HJ. A bioengineering analysis of force actions at the knee in normal and pathological gait. *Biomed Eng* 1976; **11**: 167-72.
6. Andriacchi TP, Hampton SJ, Schultz AB, Galante JO. Three-dimensional coordinate data processing in human motion analysis. *J Biomech Eng* 1979; **101**: 279-83.
7. Mann RW, Antonsson EK. Gait analysis: precise, rapid, automatic, 3-D position and orientation; kinematics and dynamics. *Bull Hosp Joint Diseases Orthop Inst* 1983; **XLIII**: 137-46.
8. Kadaba MP, Ramakrishnan, HK, Wootten ME. Measurement of lower extremity kinematics during level walking. *J Orthop Res* 1990; **8**: 383-92.
9. Cappelzo A, Leo T, Pedotti A. A general computing method for the analysis of human locomotion. *J Biomech* 1975; **8**: 307-20.
10. Andriacchi TP, Andersson GBJ, Fermier RW, Stern D, Galante JO. A study of lower-limb mechanics during stair-climbing. *J Bone Joint Surg* 1980; **62-A**: 749-57.
11. Kadaba MP, Wootten ME, Ramakrishnan HK, Hurwitz D, Cochran GVB. Assessment of human motion with vicon. In: *Proc 1987 Biomechanics Symposium, ASME, Cincinnati, Ohio, 1987*.
12. Kadaba MP, Ramakrishnan HK, Wootten ME, Gainey J,

- Gorton G, Cochran GVB. Repeatability of kinematic, kinetic, and electromyographic data in normal adult gait. *J Orthop Res* 1989; 7: 849–60.
13. Ramakrishnan HK, Kadaba MP, Wootten ME. Lower extremity joint moments and ground reaction torque in adult gait. In: *Biomechanics of Normal and Prosthetic Gait, Proc Winter Annual Meeting ASME*, Boston, Massachusetts 1987; 87–92.
14. Apkarian J, Naumann S, Cairns B. A three-dimensional kinematic and dynamic model of the lower limb. *J Biomech* 1989; 22: 143–55.
15. Whittle MW, Jefferson RJ. Functional biomechanical assessment of the Oxford meniscal knee. *J Arthroplasty* 1989; 4: 231–43.
16. Lafortune MA, Cavanagh PR, Sommer HJ III, Kalenak A. Three-dimensional kinematics of the human knee during walking. *J Biomech* 1992; 25: 347–57.
17. Chao EYS. Justification of triaxial goniometer for the measurement of joint rotation. *J Biomech* 1980; 13: 989–1006.
18. Grood ES, Suntay WJ. A joint coordinate system for the clinical description of three-dimensional motion: application to the knee. *J Biomech Eng* 1983; 105: 136–44.
19. Tupling SJ, Pierrynowski MR. Use of Cardan angles to locate rigid bodies in three-dimensional space. *Med Biol Eng Comput* 1987; 25: 527–32.
20. Kinzel GL, Hall AS Jr, Hillberry BM. Measurement of the total motion between two body segments – I: analytical development. *J Biomech* 1972; 5: 93–105.
21. Hart RA, Mote CD Jr, Skinner HB. A finite helical axis as a landmark for kinematic reference of the knee. *J Biomech Eng* 1991; 113: 215–22.
22. Deluzio KJ, Wyss UP, Li J, Costigan PA. The validation of a three-dimensional dynamic assessment system. *J Biomech* 1993; 26: 753–9.
23. Costigan PA, Wyss UP, Deluzio KJ, Li J. Semi-automatic 3-D knee motion assessment system. *Med Bio Eng Comput* 1992; 30: 343–50.
24. Siu D, Cooke TDV, Broekhoven LD, Lam M, Fisher B, Saunders G, Challis TW. A standardized technique for lower limb radiography. *Investig Radiology* 1991; 26: 71–7.
25. Andrews JG. On the specification of joint configurations and motions. *J Biomechanics* 1984; 17: 155–8.
26. Li J, Wyss UP, Deluzio KJ, Costigan PA. Three-dimensional knee joint reaction forces during walking and stair-climbing. In: *Proc 14th Annual Meeting of the American Society of Biomechanics*, Miami, Florida, 1990, 35–6.
27. Kane TR, Likins PW, Levinson DA. *Spacecraft Dynamics*. New York: McGraw-Hill, 1983.
28. Winter DA. *Biomechanics of Human Movement* (2nd edn). New York: John Wiley & Sons, 1990.
29. McConville JT, Churchill TD, Kaleps I, Cuzzi J. *Anthropometric Relationships of Body and Body Segment Moments of Inertia*, AFAMRL Technical Report 80-119 (NTIS No. AD-A097-238). Ohio: Wright-Patterson Air Force Base: 1980.
30. Clauser EC, McConville JT, Young JW. *Weight, Volume, and Center of Mass of Segments of the Human Body*. AMRL Technical Report 69-70 (NTIS No. AD-710-622). Ohio: Wright-Patterson Air Force Base, 1969.
31. *WATSMART Manual*. Northern Digital, 1989.
32. Isacson J, Gransberg L, Knutsson E. Three dimensional electrogoniometric gait recording. *J Biomech* 1986; 19: 627–35.
33. Chao EYS, Laughman RK, Schneider E, Stauffer RN. Normative data of knee joint motion and ground reaction forces in adult level walking. *J Biomech* 1983; 16: 219–33.
34. Winter D A. Biomechanical patterns in normal walking. *J Motor Behav* 1983; 15: 302–30.
35. Pennock GR, Clark KJ. An anatomy-based coordinate system for the description of the kinematic displacements in the human knee. *J Biomech* 1990; 23: 1209–18.
36. Advani HK, Harkness JG. *Day to Day Repeatability of Motion Analysis* [Unpublished Undergraduate Thesis]. Kingston, Canada: Queen's University, 1991.
37. Winter DA. *Biomechanics and Motor Control of Human Gait: Normal, Elderly and Pathological* (2nd edn). Waterloo, Ontario: University of Waterloo Press, 1991.
38. Nietert M. Das Kniegelenk des Menschen als biomechanisches Problem. *Biomedizinische Technik* 1977; 22 (1–2): 13–21.
39. Li J. *An Integrated Gait Analysis System (QGAIT) for Evaluation of Individual Loading Patterns at Knee Joint during Gait* [PhD Thesis]. Kingston, Canada: Queen's University, 1992.
40. Spitzbart A. *Analytic Geometry*. Glenview, Illinois: Scott, Foresman, 1969.

## APPENDIX A. EQUIVALENCE OF CARDAN ANGLE SET AND FLOATING-AXIS ANGLE SET

Figure 8 shows the femur and tibia in space. Both bones may actually be moving; however, for the purpose of studying the relative joint motion, the femur is usually considered fixed and the tibia is assumed to move relative to it. A right-handed Cartesian coordinate system is attached to each of the bones. The relative motion between the femur and tibia is commonly investigated by the following two methods.

1. *Cardan angle approach.* The Cardan angle set was presented by Tupling and Pierrynowski<sup>19</sup>. Initially, let the tibia rotate about  $Y_m$  through an angle  $\alpha$ , then about the rotated  $X_m$  through an angle  $\beta$ , and finally about the twice rotated  $Z_m$  through an angle  $\gamma$ . If coordinate axes in both systems are known, three angles can be calculated as:

$$\beta = \arcsin(-Y_f \cdot Z_m)$$

$$\alpha = \arcsin(X_f \cdot Z_m / \cos \beta)$$

$$\gamma = \arcsin(Y_f \cdot X_m / \cos \beta)$$

2. *Floating-axis approach.* The floating-axis system proposed by Grood and Suntay<sup>18</sup> is composed of three axes; two of them, called body-fixed axes, are the  $-Y_f$  of the femur, and  $Z_m$  of the tibia. The third axis, which is the common perpendicular to the two body-fixed axes, is referred to as the floating axis because it is not fixed in either body and moves in relation to both. The direction of the floating axis is

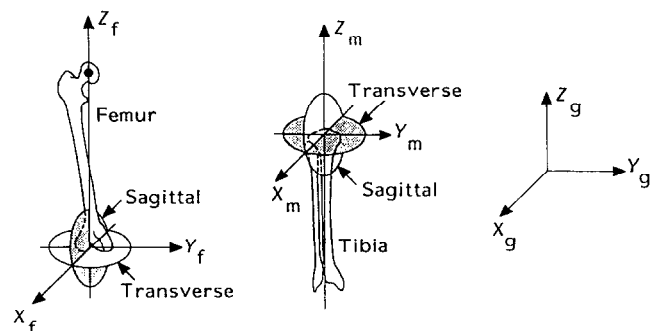


Figure 8 Illustration of the femur and tibia in space. Two body-fixed coordinate systems and the global system are shown

$F = Z_m \times (-Y_f)$ . The unit vector of  $F$  is  $\vec{e}_2$ , which is equal to:

$$\vec{e}_2 = \frac{Z_m \times (-Y_f)}{|Z_m| |Y_f| \sin \delta}$$

where  $\delta$  is the angle between  $Z_m$  and  $Y_f$ . The three rotation angles, which also represent the three clinical angles, can be calculated as follows:

$$\begin{aligned} \text{Flexion (positive)} &= \alpha & \sin \alpha &= -\vec{e}_2 \cdot Z_f \\ \text{Adduction} &= \beta - \pi/2 & \cos \beta &= -Y_f \cdot Z_m \end{aligned}$$

$$\text{External rotation (positive)} = \gamma \quad \sin \gamma = -\vec{e}_2 \cdot (-Y_m)$$

These three angles are virtually the same as the Eulerian angles defined by Chao<sup>17</sup>. The major advantage of this set of angles over the Cardan or Euler angle sets defined previously is its sequence independence nature. However, it will be shown that these angles can be expressed interchangeably with the Cardan (or Euler) angles.

**3. Equivalence of Cardan angle set and floating-axis angle set.** Cardan angles are sequence dependent; their values vary depending on different sequences of rotation axes. For the particular sequence that Tupling and Pierrynowski proposed, the first axis of rotation  $Y_m$  is coincident with the flexion-extension axis of the floating-axis system,  $Y_f$ , before the rotation. In the second stage the intermediate axis  $X_m$  is the same as the floating axis  $e_2$ , which is perpendicular to both the  $Y_f$  and the forthcoming third rotation axis  $Z_m$ .  $Z_m$  is obviously the same in both systems.

To evaluate the values for each angle, assume three Cardan angle values are  $\alpha_c$ ,  $\beta_c$  and  $\gamma_c$ , three floating-axis angle values are  $\alpha_f$ ,  $\beta_f$  and  $\gamma_f$ . Since the angle between the  $Y_f$  and  $Z_m$  is  $\beta_f$ , and both  $Y_f$  and  $Z_m$  are unit vectors, vector  $\vec{e}_2$  can be rewritten as:

$$\vec{e}_2 = -\frac{Z_m \times Y_f}{\sin \beta_f} \quad (4)$$

First compare abduction-adduction angles,  $\beta_c = \arcsin(-Y_f \cdot Z_m)$  and  $\beta_f = \arccos(-Y_f \cdot Z_m)$ , so  $\beta_c = \pi/2 - \beta_f$ . For the flexion-extension angles:

$$\begin{aligned} \sin \alpha_f &= \vec{e}_2 \cdot Z_f = \frac{Z_m \times Y_f \cdot Z_f}{\sin \beta_f} \\ &= \frac{Z_m \cdot Y_f \times Z_f}{\sin \beta_f} = \frac{Z_m \cdot X_f}{\cos \beta_c} = \sin \alpha_c \end{aligned} \quad (5)$$

Equation (5), which used equation (1), (3), (4) and triple vector product properties<sup>40</sup>, leads to  $\alpha_c = \alpha_f$ . A similar approach can be followed to show that  $\gamma_c = -\gamma_f$ . The minus sign occurs because internal rotation is positive in the Cardan angle definition while external rotation is positive in the floating-axis definition. In summary, for the particular Cardan angle sequence of rotation, Cardan and floating-axis angles can be expressed in terms of each other. In kinematic analysis, either can be used to describe the three-dimensional orientation of a joint.

## APPENDIX B. GOVERNING EQUATIONS

Two governing equations used to calculate the net reaction forces and external moments are:

$$F_j = ma_{cm} - F_G + mg \quad (6)$$

$$M_N = -\dot{H} + M_G + M_j$$

where

$F_j$  = joint reaction force at the knee joint

$m$  = mass of the foot and shank

$a_{cm}$  = acceleration of the centre of mass

$F_G$  = ground reaction force

$g$  = gravity acceleration

$M_N$  = net external moment about the centre of mass

$M_G$  = moment of ground reaction force about the centre of mass

$M_j$  = moment of joint reaction force about the centre of mass

$H_{cm}$  = angular momentum about the centre of mass

Note that the forces are easier to calculate in the global coordinate system since all force vectors on the right-hand side of the equations are estimated in the global system. It is easier, however, to calculate the moments with respect to the body-fixed coordinate axes since these axes are the principal inertia axes of the foot and shank. Therefore, components of the first derivative of angular momentum  $H_{cm}$  can be expressed using Euler equations:

$$\begin{aligned} \dot{H}_1 &= I_{11} \dot{\omega}_1 - (I_{11} - I_{33}) \omega_2 \omega_3 \\ \dot{H}_2 &= I_{11} \dot{\omega}_2 - (I_{33} - I_{11}) \omega_1 \omega_3 \\ \dot{H}_3 &= I_{33} \dot{\omega}_3 \end{aligned} \quad (7)$$

If moments are calculated about the knee joint rotation centre  $k$ , the moment-governing equation will be in a different form:

$$M_N = -\dot{H}_k + r_{kc} \times ma_k + M_G - M_g$$

Where  $r_{kc}$  is the vector from the joint-rotation centre of the centre of mass and  $a_k$  is the acceleration of the joint centre  $k$ .  $M_g$  is the moment by gravity force of the segment mass about the knee-joint centre. Comparing (8) with (6),  $M_j$  disappears since  $F_j$  passes through the joint-rotation centre  $k$ . The additional term  $r_{kc} \times ma_k$  can only be ignored in the following three situations:

1.  $k$  is fixed;
2.  $k$  is the mass centre;
3.  $k$  is moving with the constant velocity.

As the instant centre of the shank relative to the femur, the knee-joint rotation centre does not fall into any of these three categories. Therefore, two different equations should be employed when using two different moment balance points.